AAS 13-438

PRECISION LANDING AT MARS USING DISCRETE-EVENT DRAG MODULATION

Zachary R. Putnam* **and Robert D. Braun†**

An entry, descent, and landing architecture capable of achieving Mars Science Laboratory class landed accuracy (with 10 km of target) while delivering a Mars Exploration Rover class payload to the surface of Mars is presented. The architecture consists of a Mars Exploration Rover class aeroshell with a rigid, annular drag skirt. Maximum vehicle diameter is limited to be compatible with current launch vehicle fairings. A single drag skirt jettison event is used to control range during entry. Three-degree-of-freedom trajectory simulation is used in conjunction with Monte Carlo techniques to assess the flight performance of the proposed architecture. Results indicate landed accuracy is competitive with pre-flight Mars Science Laboratory estimates, and peak heat rate and integrated heat load are significantly reduced relative to the Mars Exploration Rover entry system. Modeling parachute descent within the onboard guidance algorithm is found to remove range error bias present at touchdown; the addition of a range-based parachute deploy trigger is found to significantly improve landed accuracy.

INTRODUCTION

Over the past several decades, NASA has compiled an impressive record of successful missions to the surface of Mars. However, landing payloads of useful size at scientifically interesting locations on the surface of Mars remains a significant challenge.[1] For example, the Mars Science Laboratory (MSL) mission required a complex entry, descent, and landing (EDL) system to meet modest landed accuracy and altitude requirements for a payload of approximately one metric ton.[2] The MSL EDL system utilized a lifting aeroshell, a reaction control system (RCS), and a bank-to-steer guidance, navigation, and control system to achieve the required terminal accuracy and maintain altitude margin for terminal descent. Lifting, bank-to-steer hypersonic trajectory control systems have been used with success in the past at Earth for blunt-body entry vehicles with landed accuracy requirements, most notably in the Gemini, Apollo, and Soyuz programs. MSL was the first demonstration of such a system at Mars. Bank-to-steer systems provide good terminal accuracy, but add significant complexity, mass, and cost to an EDL system. All bank-to-steer systems to date have required a RCS with its associated thrusters, propellant, tanks, and plumbing; an off-centerline center of gravity (c.g.) position to produce the required lift; and an onboard guidance, navigation, and control system. In addition to the cost, mass, and complexity of these systems, including design, manufacture, and test, bank-to-steer subsystems may also impact other EDL subsystems. For MSL, these subsystem impacts required the use of two sets of ballast masses and their associated jettison events to control c.g. position during the mission[2] and extensive study of aerothermodynamic jet-interaction effects in the hypersonic flow regime around the vehicle.[3]

*Graduate Research Assistant, School of Aerospace Engineering, Georgia Institute of Technology, 270 Ferst Drive, Atlanta, GA, 30332.

†Professor, School of Aerospace Engineering, Georgia Institute of Technology, 270 Ferst Drive, Atlanta, GA, 30332.

This study presents a simpler EDL architecture for precision landing on the surface of Mars: discrete-event, drag-only trajectory control, achieved through a one-time drag area jettison event. The jettison event instantly changes the vehicle ballistic coefficient, β.* β is defined by Eq. (1), and may be thought of as the ratio of inertial to aerodynamic forces. The jettison event adjusts the ratio of inertial to aerodynamic forces by changing β so that the desired range is flown. The timing of this event is selected in real time by the onboard guidance system using available navigation data. This architecture does not require any vehicle attitude maneuvers during EDL, eliminating the need for a RCS on the entry vehicle. Additionally, since no lift is required, no c.g. offset is used and the vehicle c.g. may remain on centerline through all mission phases. The ejectable drag area may be rigid and deployed prior to launch.

$$\beta = \frac{m}{C_D S_{ref}} \tag{1}$$

While drag modulation as a means of trajectory control for EDL systems is not a new idea, only a limited number of studies on drag modulation are available in the literature. Levy determined a closed-form solution using drag modulation to limit the rate of increase of deceleration during entry.[4] Rose and Hayes evaluated drag modulation as means for orbit phasing and entry targeting.[5] Kuo et al. examined the use of drag modulation to track reference trajectories for ballistic missiles.[6] These studies all assumed drag could be controlled continuously within a given interval. Discrete-event drag modulation has been studied for planetary aerocapture missions at the conceptual level;[7,8,9] but only a few studies address realistic guided system performance.[10,11,12] This study seeks to extend discrete-event drag modulation systems to EDL at Mars.

The goal of this study is to show that MSL-class landed accuracies (landing within 10 km of a target) is feasible for a Mars Exploration Rover (MER) class entry mass (830 kg) using discrete-event drag modulation with a rigid drag skirt whose maximum diameter is restricted to be compatible with current launch vehicle fairing diameters. The analyses presented focus on trajectory performance, including terminal accuracy, peak deceleration, peak heat rate, integrated heat load, and parachute deploy conditions.

SYSTEM CONCEPT

An EDL architecture is envisioned which is capable of delivering an MER-class payload to the surface of Mars with MSL-class accuracy using discrete-event drag modulation. The simplest method of drag modulation is utilized: a one-time discrete change in drag area, achieved by jettisoning a rigid, annular forebody heat shield skirt. The jettison point is selected in real time by the onboard guidance algorithm, using inertial measurement unit (IMU) measurements, to achieve the desired range; crossrange errors are not controlled.

Vehicle Configuration

The proposed EDL architecture is comprised of four major parts: a MER-class aeroshell, a rigid annular heat shield extension, a 14 m diameter MER-class supersonic disk-gap-band (DGB) parachute,[1] and an airbag landing system. The MER-class aeroshell is a 2.65 m diameter 70-deg sphere cone with a nose radius of 0.66 m.[13] The rigid heat shield extension, or drag skirt, is shaped to maintain the 70-deg sphere cone geometry while increasing the outer diameter from 2.65 m to

*A section on mathematical notation is provided in the sequel.

4.5 m. This outer diameter allows the vehicle to fit within current 5 m diameter launch fairings in its entry configuration (see Figure 1), eliminating the need for in-space deployment events prior to atmospheric entry at Mars. The total vehicle entry mass is 950 kg, composed of an 830 kg MER entry vehicle and a 150 kg drag skirt. The mass of the drag skirt was approximated using the areal mass of the MER heat shield. This drag skirt mass estimate is likely conservative, because the skirt is not part of the primary structure or load path, and because heat rates are significantly lower for this EDL architecture relative to MER. Jettison of the drag skirt is accomplished by three sets of redundant pyrotechnic separation bolts. The MER-sized aeroshell β is significantly higher than the three expended drag skirt segments, aiding in performance of a reliable separation and decreasing re-contact risk.

Drag skirt jettison and parachute deploy are commanded by the onboard guidance, navigation, and control system. The navigation system is anticipated to be a strap-down inertial system, with a state update provided immediately prior to entry by the Deep Space Network (DSN) using standard high-accuracy state determination techniques, such as Delta Differenced One-way Range measurements.[14] Prototype guidance and targeting algorithms are discussed below.

The entry sequence for the system concept is shown in Figure 2. Prior to entry interface (EI), a final navigation state update is received from the DSN and the cruise stage is jettisoned. The vehicle then enters the atmosphere and begins the low-β deceleration phase. The onboard guidance algorithm determines when to jettison the rigid heat shield skirt based on onboard IMU data. Peak heating and peak deceleration may occur either before or after jettison depending on day-of-flight dispersions. At jettison, the vehicle β immediately rises. The vehicle continues to decelerate in the high-β phase to the proper parachute deploy conditions. The supersonic parachute is then deployed and the vehicle descends to terminal descent initiation and touchdown.

Real-time Guidance and Targeting Algorithm

During atmospheric entry, the onboard guidance algorithm uses data from the navigation system to determine when to jettison the drag skirt and deploy the parachute. This strategy allows the vehicle to select the proper jettison and deploy points based on day-of-flight conditions. Three different modes of the guidance algorithm were evaluated (see Figure 3). Mode 1 targets the parachute deploy point. Mode 2 models the parachute descent phase, enabling the algorithm to target the touchdown point. For modes 1 and 2, the parachute is deployed at a preset velocity. Mode 3 uses a range-based parachute deploy trigger to reduce range error at touchdown, effectively creating a two-stage drag modulation system.

After EI, the guidance algorithm begins targeting once the sensible atmosphere has been reached, defined by sensed accelerations greater than 0.5 m/s^2. Targeting is performed with a numeric predictor-corrector (NPC). The NPC determines the drag skirt jettison time that nulls the terminal range error, subject to a minimum velocity jettison limit. This minimum jettison velocity is chosen to provide a minimum of 60 m/s between jettison and parachute deploy. Guidance execution terminates after parachute deploy.

The guidance target is input as a set of geodetic latitude-longitude coordinates. At initialization, these coordinates are transformed into a planet-centered inertial position vector. Current target position is then estimated based on the initial target position, the estimated time of flight computed by the predictor, and the planet rotation rate.

The guidance predictor models Mars as an oblate spheroid with inverse-square gravity includ-

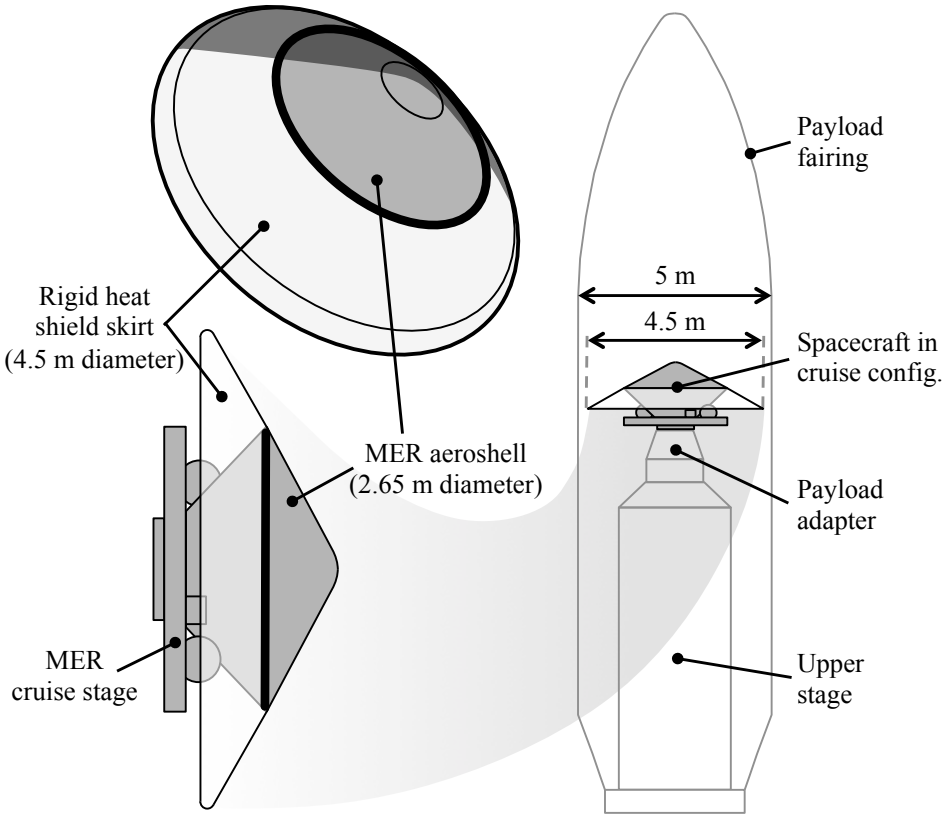

Figure 1. The system concept consists of a MER-class aeroshell and cruise stage with a rigid heat shield extension; the concept fits within a standard 5 m launch fairing.

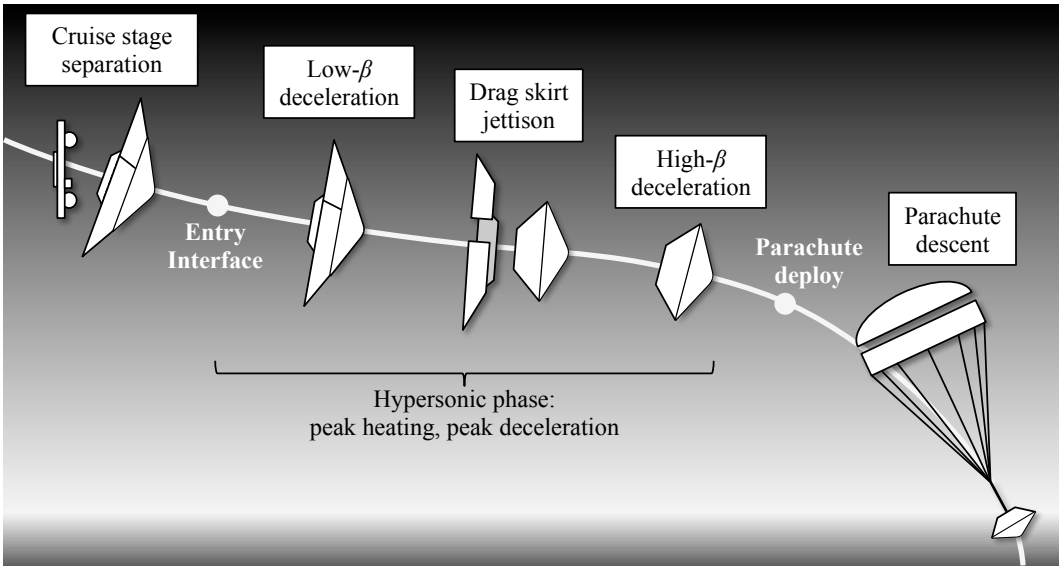

Figure 2. Discrete-event drag modulation concept EDL sequence.

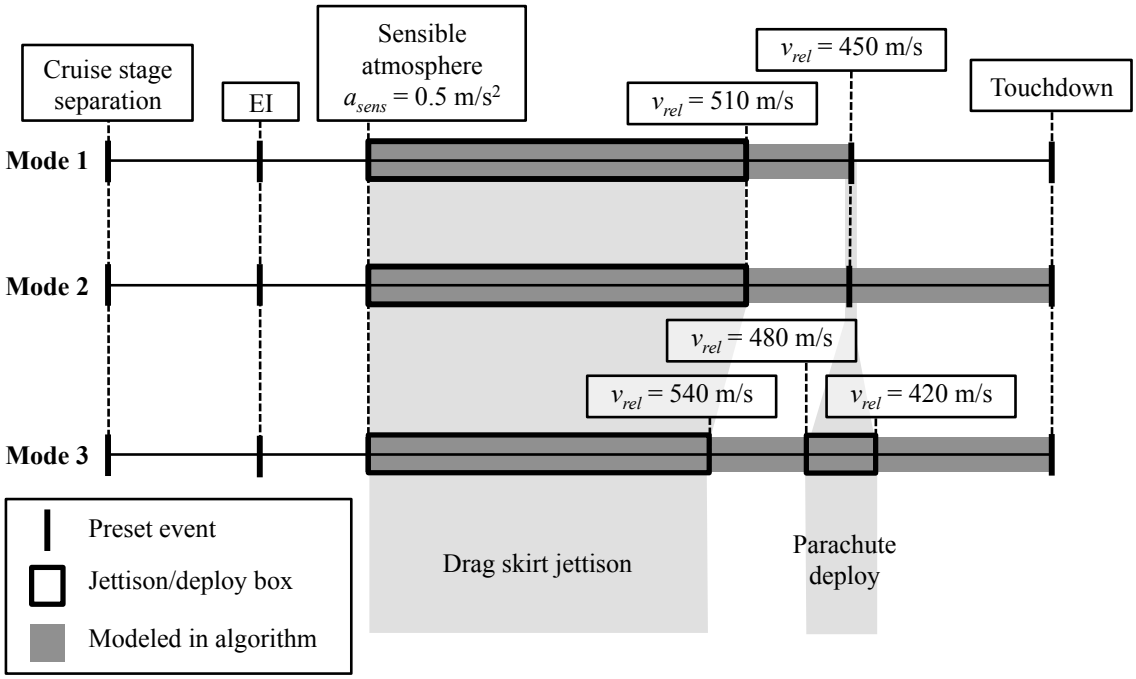

Figure 3. Guidance and targeting modes.

ing J2 oblateness effects and a nominal altitude-density atmosphere table. The vehicle is modeled as a point mass that generates only drag. Vehicle and parachute drag are modeled with constant C_D values. The predictor integrates the three-degree-of-freedom equations of motion using a 4th-order Runge-Kutta method. While the bulk of the integration is performed with a constant time step of 1 s, the time steps immediately adjacent to the jettison event are adjusted such that the jettison occurs a major integration step. This method enhances the accuracy and stability of the prediction without significantly increasing the computational time. Protection is provided for off-nominal cases through a integration time limit and minimum and maximum altitude bounds. For mode 1, prediction is terminated at parachute deploy. For modes 2 and 3, the predictor models the parachute descent phase assuming a preset parachute deploy velocity and terminates at touchdown. For mode 3, after drag skirt jettison, the predictor continues to run, terminating at touchdown, but the parachute is now deployed at a velocity determined by the corrector.

In all three algorithm modes, the corrector utilizes the terminal states computed by the predictor to determine when the drag skirt should be jettisoned to satisfy the terminal range error tolerance. First, the corrector computes the terminal range error from the estimated target position and the predicted terminal vehicle position. If the computed range error is less than the tolerance, the jettison time and corresponding range error are stored and the NPC terminates. If the range error is greater than the tolerance and no previous (jettison time, range error) prediction pairs exist, the corrector adjusts the jettison time in the direction of the range error and recomputes the range error with the updated jettison time estimate. If the range error is greater than the tolerance, and a previous prediction pair exists, the corrector attempts to jump to the solution using a linear fit of the two available points. The linear curve fit computation includes divide-by-zero protection. The predictor is then re-run with the updated jettison time. This process repeats until either the range error tolerance is satisfied or the NPC iteration limit is reached. For mode 3, a similar corrector algorithm is used after drag

skirt jettison to determine the parachute deploy velocity that nulls the range error at touchdown.

The guidance algorithm estimates a constant-bias atmospheric density correction factor at the start of each guidance cycle. This estimation accounts for day-of-flight variability in the Mars atmosphere and is required to achieve accurate terminal state predictions. The correction factor is computed from navigated acceleration and velocity and an onboard table look-up atmosphere model. The current estimate of the density is determined from Eq. (2), where a_{axial} is the acceleration due to drag in the axial direction and v_{wind} is the magnitude of the wind-relative velocity vector. Neither of these quantities are available directly in the absence of a flush air data system, so they are approximated with the sensed acceleration magnitude and the planet-relative velocity magnitude, respectively. The density correction factor relative to the onboard model is then computed. Using a factor allows the predictor to update the onboard atmosphere model by multiplying it by a constant parameter. To improve the estimate, the factor is limited to minimum and maximum values and filtered with previous values using a low-pass filter. A filter gain of 0.05 provides a balance between reducing noise and capturing short-period changes in the atmosphere relative to the onboard model. The bounded, filtered estimate is then stored for use by the predictor.

$$\rho_{est} = \frac{2ma_{axial}}{v_{wind}^2 S_{ref} C_A} \tag{2}$$

Two different parachute deploy triggers were evaluated: a velocity trigger (modes 1 and 2) and a range-based trigger (mode 3). The velocity trigger deploys the parachute at a pre-set planet-relative velocity of 450 m/s. This type of trigger was used on the Phoenix and MSL missions.[15] The deploy velocity was selected to ensure compliance with the MER DGB parachute deployment box.[16] The range-based trigger utilizes the predictor-corrector discussed above to determine the parachute deploy velocity which minimizes the range error at touchdown. The range-based trigger deploy velocity is restricted to values between 420 and 480 m/s. The lower velocity bound was selected to ensure at least 70 s were available for terminal descent, similar to Mars Pathfinder.[17,18] The upper velocity was selected to limit Mach number and dynamic pressure at deploy to the MER parachute deployment box.[16]

The algorithm is run at 0.5 Hz to minimize its computational load on the flight computer. Guidance parameters may be adjusted to reduce the computational resource requirements of the algorithm as required, including the call rate, internal iteration limit, the nominal prediction time step, and the size of the onboard atmosphere table. Future design studies should examine trade-offs with respect to these settings between improved performance at higher rates and fidelities and reduced computational load at lower rates and fidelities.

METHODS AND ASSUMPTIONS

Trajectory Simulation

A three-degree-of-freedom trajectory simulation was used to evaluate flight performance of the proposed EDL system concept. The simulation is written in Matlab and is autocoded to C and compiled to improve execution speed. A constant time step 4th-order Runge-Kutta technique is used to integrate the equations of motion at 100 Hz.

Table 1 summaries the relevant parameters used to characterize the Mars environment. The Mars atmosphere is modeled using Mars-GRAM 2010.[19] Atmospheric data is generated as a function

Table 1. Mars Properties

Property	Value
Equatorial radius	3396.2 km
Polar radius	3376.2 km
Gravitational parameter	4.283×10^{13} $\mathrm{m}^3/\mathrm{s}^2$
J2 perturbation	1.9605×10^{-3}
Mars-GRAM date, time	6 August 2012, 5:17 UTC
Mars-GRAM dusttau	0.3
Ratio of specific heats	1.2941
Sutton-Graves coefficient	1.898×10^{-4} $\mathrm{kg}^{0.5}$/m

of altitude at the equator for the same day MSL landed using default Mars-GRAM settings. The surface of Mars is modeled as an oblate spheroid. Gravity is modeled as an inverse-square relation with J2 oblateness effects. Convective stagnation point heat rates are estimated using the Sutton-Graves relation.[20] Radiative heating is assumed to be negligible for the entry velocities and energies considered in this study.[21]

The vehicle is modeled as a point mass. The drag skirt jettison event is accompanied by a step change in the vehicle mass and aerodynamic reference area. Tables of aerodynamic coefficients were generated for a 70-deg sphere cone as a function of Mach number and angle-of-attack using CBAero.[22] The aerodynamic coefficients are assumed to be constant across the jettison event, since the overall shape of the vehicle remains a 70-deg sphere cone, although aerodynamic forces change drastically due to the reduction in aerodynamic reference area. The vehicle is given a constant 2 RPM bank rate to mitigate the integrated effects from lift generated by potential off-centerline c.g. positions. The MER aeroshell nose radius of 0.66 m is used to compute stagnation point heating rates.[13] The parachute drag coefficient is computed as a function of Mach number using data from the MSL program.[23] Parachute inflation is not modeled; parachute deployment is considered to be instantaneous. Terminal descent and impact attenuation systems are not modeled.

The vehicle flight computer is modeled as collection of rate-differentiated processes. Navigation is run at 40 Hz; the navigation model computes vehicle state information used by guidance and flight control. Guidance runs at 0.5 Hz; it determines the time at which the drag skirt jettison and parachute deployment should occur. Flight control runs at 20 Hz; it continuously checks drag skirt jettison, and then parachute deploy, criteria and issues the jettison and deploy commands when the criteria are satisfied.

The navigation system is modeled as a Markov process. The model generates navigation errors that would be observed if the navigation system performed according to a given set of navigation accuracy requirements. The Markov-process random variable is given by Eq. (3), where Δt is the time between measurements; τ is the time constant, set to 3600 seconds for this model; and η_i is the noise magnitude at a given time step.

$$x_{i+1} = e^{\left(\frac{-\Delta t}{\tau}\right)} x_i + \eta_i \tag{3}$$

The incremental error at a given time step, $\mathbf{e}_i$, is then given by Eq. (4), where $\mathbf{P}_{SS}$ is the steady-state error covariance matrix, defined by the required navigation system performance and $\mathbf{x}_i$ is a vector of Markov-process random variables.

$$\mathbf{e}_i = \mathbf{P}_{SS}\mathbf{x}_i \tag{4}$$

Defining η_i as shown in Eq. (5) ensures that the knowledge error in the navigation system does not exceed that defined by $\mathbf{P}_{SS}$.

$$\eta_i = 1 - e^{\left(\frac{-2\Delta t}{\tau}\right)} \tag{5}$$

The incremental errors are then applied to the inertial position, velocity, and acceleration truth state vectors generated from the equations of motion to determine the current navigated vehicle state, as shown in Eq. 6. This navigated vehicle state is then used to compute state quantities required for the guidance algorithm.

$$\begin{bmatrix} \mathbf{r} \\ \mathbf{v} \\ \mathbf{a} \end{bmatrix}_{nav,i} = \mathbf{e}_i + \begin{bmatrix} \mathbf{r} \\ \mathbf{v} \\ \mathbf{a} \end{bmatrix}_{truth,i} \tag{6}$$

Uncertainty Analysis

Monte Carlo simulation techniques were used to evaluate system performance in the presence of day-of-flight dispersions, including state, vehicle, and day-of-flight environmental uncertainties. Uncertainty models are described below; specific model parameters and inputs are given in Table 2.

Both delivery and knowledge errors were modeled. Correlated delivery error was modeled using a covariance matrix generated from MSL navigation data.[14] State knowledge error was modeled during entry using the Markov-process navigation error model discussed above. Vehicle aerodynamic properties were varied based on vehicle configuration and flight regime. Uncertainties in aeroshell aerodynamics in the supersonic and hypersonic regimes were modeled with correlated normal distributions.[24] Uncertainty in aeroshell aerodynamics in the subsonic regime was not modeled, as the subsonic aerodynamics are dominated by the parachute. Parachute drag coefficient uncertainty was modeled as a function of Mach number and a uniformly-distributed factor.[23] In addition to aerodynamic coefficients, vehicle angle of attack was dispersed about a nominal of zero degrees and the initial bank angle was dispersed with a uniform distribution over 360 degrees to account for off-centerline c.g. positions. A constant bank rate was used to mitigate the effects of non-zero angles of attack; the constant bank rate was dispersed about its nominal of 2 RPM with a normal distribution. Vehicle mass uncertainty was modeled with a normal distribution. Dispersed atmospheric data were generated using Mars-GRAM 2010.[19] The required number of dispersed atmosphere tables were generated offline and stored for use in the Monte Carlo simulation.

Range Metrics

Downrange and crossrange at the landing site were determined relative to a reference azimuth. The reference azimuth was defined to be the planet-relative azimuth angle of a nominal trajectory at parachute deploy. The reference azimuth and the target landing site define a plane; downrange is then the in-plane distance traveled over the surface of Mars during EDL and crossrange is the out-of-plane distance, both relative to the target position. Range over the surface of Mars is calculated using Vincenty's algorithm for computing geodesics.[25] Accuracy was determined by the total range error, the distance between the vehicle's position and the target landing site.

CORRIDOR DEFINITION AND DIVERT CAPABILITY

The feasibility of utilizing a discrete-event drag modulation system for trajectory control during entry at Mars was assessed using simplified models for the Mars environment: an exponential atmosphere and a spherical planet. Entry trajectories shown in this section are eastbound equatorial.

Table 2. Monte Carlo Simulation Uncertainty Model Parameters and Inputs

Parameter	Dispersion min/max or 3σ	Notes
Atmosphere	model	Mars-GRAM, default settings for 6 AUG 2012, 5:17 UTC
Hypersonic C_A	3%	Correlated with supersonic C_A[24]
Supersonic C_A	10%	Correlated with hypersonic C_A[24]
Hypersonic C_N	5%	Correlated with supersonic C_N[24]
Supersonic C_N	8%	Correlated with hypersonic C_N[24]
Parachute C_D factor	± 1	MSL DGB parachute[23]
Trim angle of attack	2 deg	Accounts for off-centerline c.g. positions
Initial bank angle	± 180 deg	Covers all possible c.g. offset orientations
Bank angle rate	5%	
Vehicle mass	2 kg	Ref. 24
EI velocity	0.65 m/s	Correlated delivery error[14]
EI flight-path	0.018 deg	Correlated delivery error[14]
EI azimuth	0.006 deg	Correlated delivery error[14]
EI latitude	0.013 deg	Correlated delivery error[14]
EI longitude	0.017 deg	Correlated delivery error[14]
EI altitude	1.17 km	Correlated delivery error[14]
State knowledge	model	Markov-process with MSL knowledge error estimate

The MER-B entry interface state is used: EI inertial velocity of 5.5 km/s and EI inertial flight-path angle of -11.47 deg.[1]

The entry corridor for the drag modulation systems is defined by two trajectories: the minimum-β trajectory, which carries the drag skirt all the way to the surface, and the maximum-β trajectory, which jettisons the drag skirt at EI. For a given entry range, the most shallow EI flight-path angle possible is achieved by the minimum-β trajectory, while the steepest possible EI flight-path angle possible is achieved by the maximum-β trajectory. The range of potential EI flight-path angles bounded by these trajectories defines the entry corridor. Figure 4 (a) and (b) show example corridor-bounding trajectories at Mars. The minimum-β trajectory decelerates higher in the atmosphere and requires a more shallow EI flight-path angle to achieve a given range. The maximum-β trajectory decelerates lower in the atmosphere and requires a more steep EI flight-path angle to achieve a given range.

From a given EI state, the maximum-β trajectory will have the longest possible entry range and the minimum-β trajectory will have the shortest possible entry range. The difference between these ranges is the total divert capability of the vehicle; jettisoning the drag skirt at different points during the trajectory will result in intermediate ranges. Figure 5(a) shows total entry range as a function of drag skirt jettison time and planet-relative velocity. Early jettisons result in a range of approximately 725 km and late jettisons result in a range of approximately 615 km, resulting in a divert capability of over 100 km. The slope of the jettison time versus range curve, $\Delta(\text{range})/\Delta(\text{jettison time})$, is the range control sensitivity at any given time. Peak control sensitivity roughly corresponds to peak deceleration (for the minimum-β entry), as shown in Figure 6. This peak occurs near the middle of the flight, indicating that jettison must be acceptable both before and after peak deceleration (and peak heating) to capitalize fully on the available range control authority. Figure 5(b) shows that the change in entry range with vehicle velocity at jettison is nearly linear. While not explored in this study, this relationship may provide an avenue for future development of a simple guidance law.

Figure 7 shows bounding minimum- and maximum-β trajectories for three atmospheric density

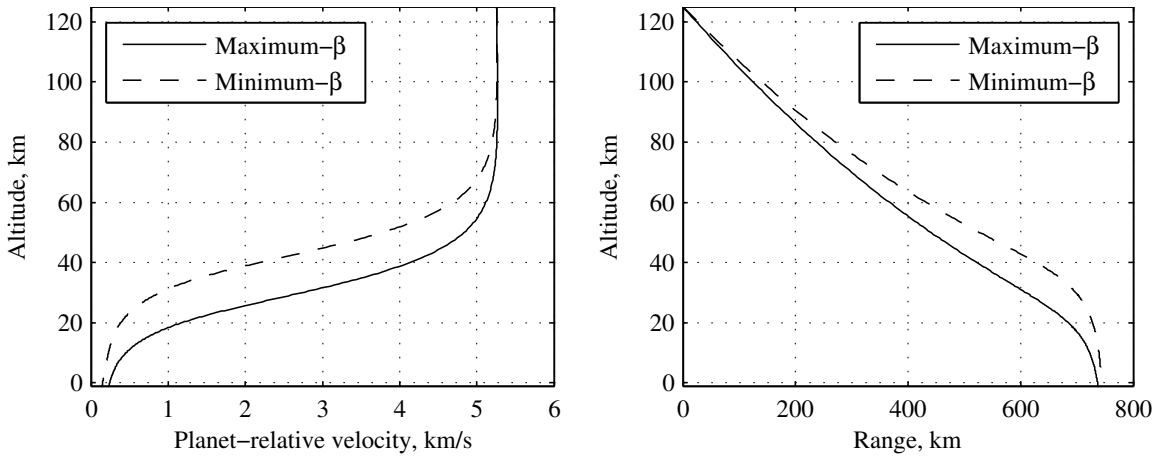

(a) Altitude versus planet-relative velocity.

(b) Altitude versus range.

Figure 4. Example corridor-bounding entry trajectories for a drag modulation vehicle at Mars.

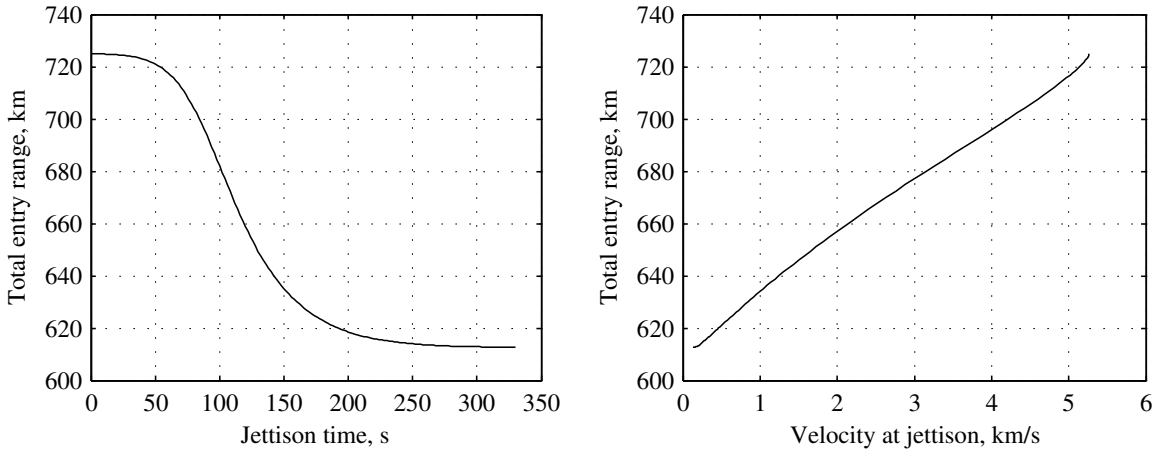

(a) Altitude versus jettison time.

(b) Range versus jettison velocity.

Figure 5. Total entry range as a function of jettison time and velocity.

biases: -30% (red), nominal (black), and $+30\%$ (blue). Each of these sets of trajectories shows that the vehicle is capable of range diverts over 100 km. More significantly, there exists a nearly 50 km range "window" between the minimum-β, low-density trajectory and the maximum-β, high-density trajectory (the two central red and blue trajectories, respectively). This provides an estimate of the remaining range control authority available under off-nominal atmospheric conditions, and indicates that discrete-event drag modulation may be feasible for entry at Mars.

EDL PERFORMANCE

Mission Design

The EI state and target landing site used for the rest of this study are given in Table 3. The landing site corresponds to Gale Crater, MSL's landing site. The EI state was selected to match the velocity of the MER-B entry. The EI flight-path angle was selected to be more shallow than MER-B's value

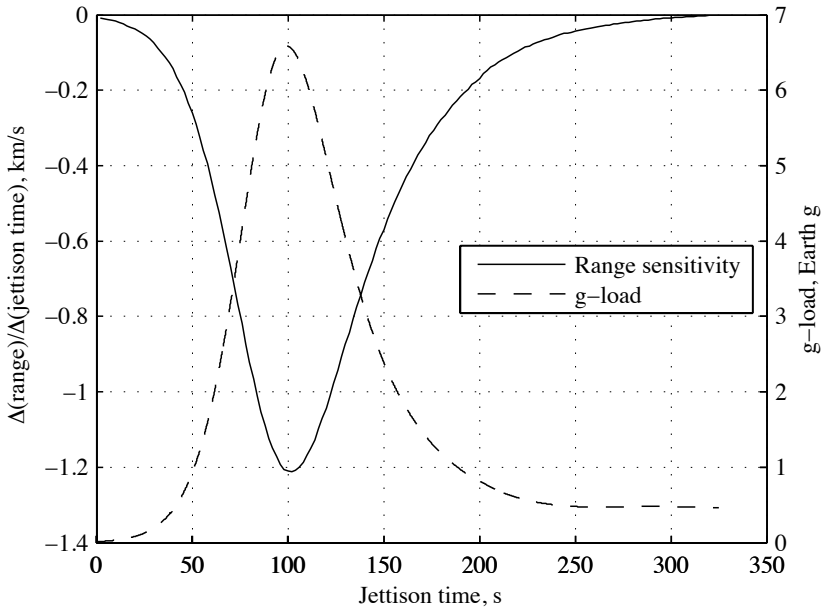

Figure 6. Change in total entry range as a function of drag skirt jettison time; nominal g-load at jettison time.

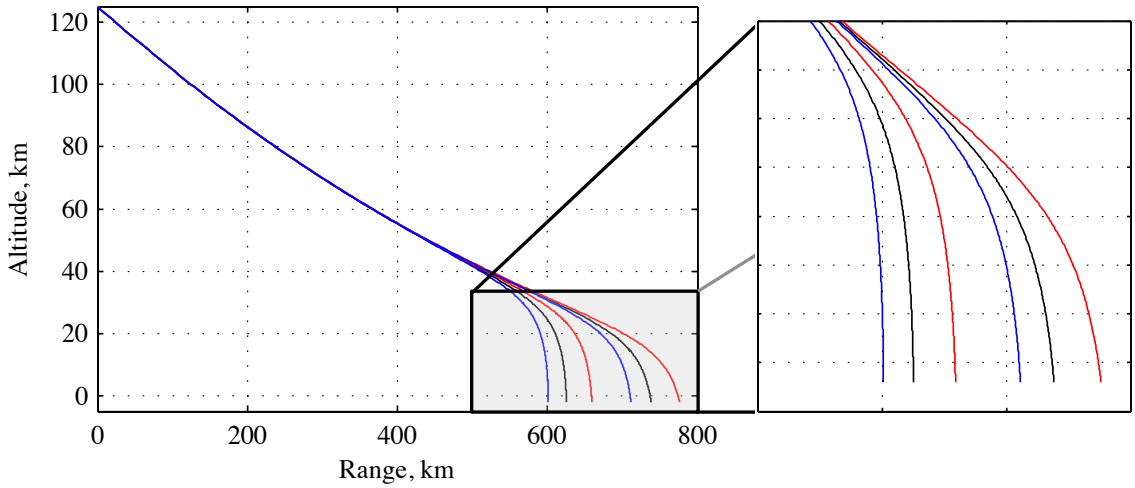

Figure 7. Altitude versus downrange for corridor-bounding trajectories over three different density profiles.

of -11.47 deg to accommodate the lower initial β of the proposed EDL architecture. The EI latitude and longitude were selected to line up the EI point with the target landing site while maintaining an initial azimuth of 45 deg. For this EI-target pair, the flight range is approximately 900 km.

The selection of the initial position is critical and places a constraint on interplanetary navigation performance, since drag modulation vehicles have no out-of-plane (crossrange) control authority. The EI state error can be tailored to reduce specific initial state errors;[26] this strategy should be used to minimize initial crossrange and azimuth errors for drag modulation EDL systems to minimize the effect of their lack of out-of-plane control authority on terminal accuracy.

Table 3. Trajectory Parameters

Item	Parameter	Nominal value
Entry interface state	Altitude	125 km
	Geodetic latitude	-16.258 deg N
	Longitude	127.165 deg E
	Inertial velocity magnitude	5.5 km/s
	Inertial flight-path angle	-11.0 deg
	Inertial azimuth	45 deg
Target	Altitude	-1.5 km
	Latitude	-5.4 deg
	Longitude	137.7 deg

Nominal Performance

The nominal guided entry performance of the proposed EDL architecture was assessed through numeric simulation using mode 1 of the algorithm (parachute deploy target). Figure 8 shows the simulated nominal trajectory, including the trajectory of a single piece of the jettisoned drag skirt. The jettison event occurs near 175 s and the parachute is deployed at 450 m/s. After drag skirt jettison, the vehicle's higher β causes the trajectory to immediately steepen (Figure 8(a)), but also significantly reduces the sensed deceleration (Figure 8(b)). The peak hypersonic peak deceleration is approximately 6 g; while parachute opening loads reach 9 g, parachute inflation is not modeled, so this number may be inaccurate. Range error is approximately 300 m at parachute deploy, increasing to 4.7 km at touchdown. This increase in range error during parachute descent is due to the relatively shallow flight-path angle of -27 deg at parachute deploy: the vehicle still has significant horizontal velocity well into the parachute descent (Figure 8(c)).

The jettisoned drag skirt segments are conservatively assumed to have a C_D of 1.0. Post-jettison, the vehicle has a β of approximately 90 kg/m^2 and each skirt segment has a β of 15.5 kg/m^2. This difference in β between the vehicle and jettisoned skirt segments provides a favorable jettison scenario, where re-contact is unlikely, even with a conservative C_D. A higher C_D for the skirt segments would only increase the difference in β. Figure 8(d) shows that re-contact does not appear to be an issue for this trajectory.

Monte Carlo Simulation Results

Monte Carlo simulation was used to assess the performance of the proposed EDL architecture in the presence of day-of-flight uncertainties for all three guidance modes. A sample size of 1000 was used for each Monte Carlo simulation. Results are summarized in Table 4 and uncertainty inputs are given above in Table 2.

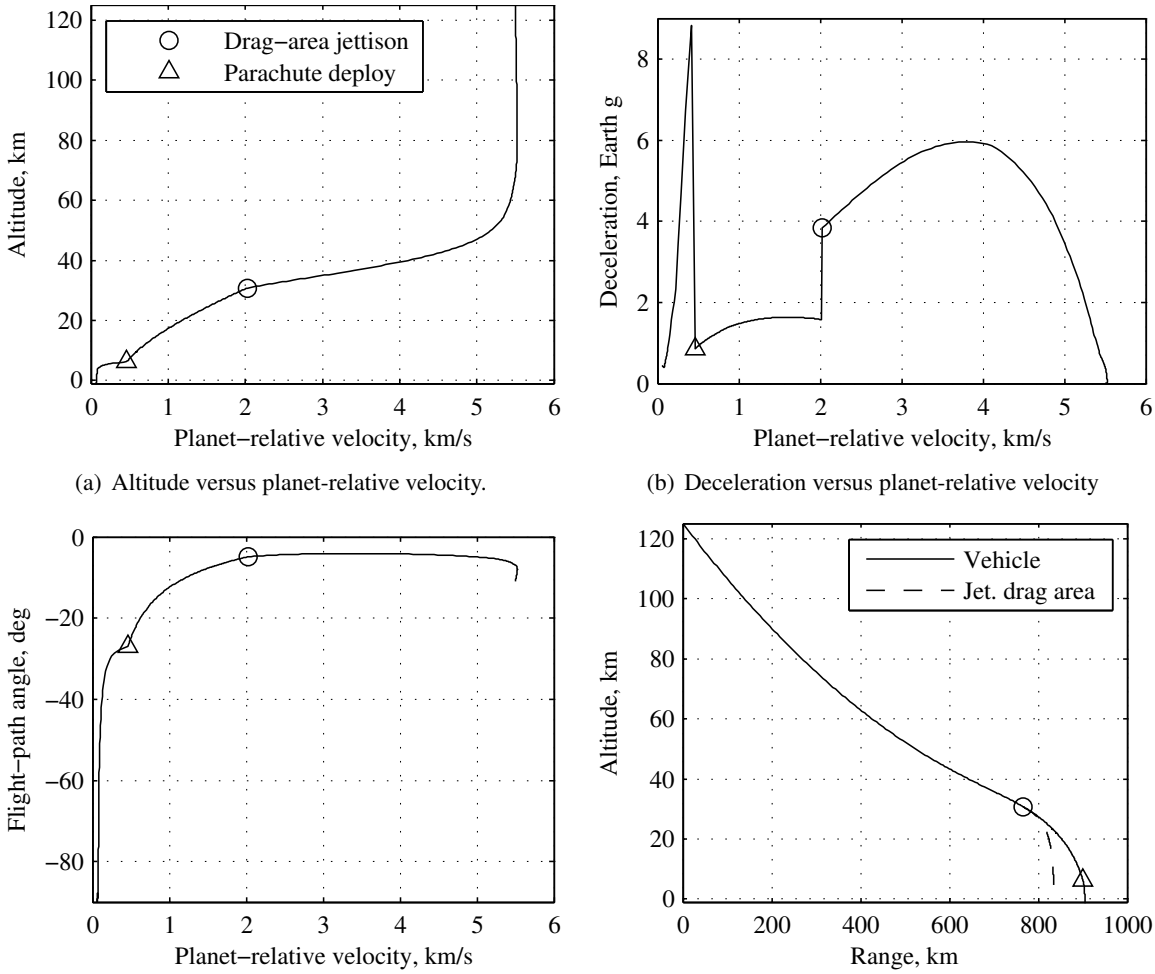

(a) Altitude versus planet-relative velocity.

(b) Deceleration versus planet-relative velocity

(c) Flight-path angle versus planet-relative velocity.

(d) Altitude versus range..

Figure 8. Nominal entry trajectory for guidance mode 1.

Figure 9 shows the nominal and dispersed entry trajectories for guidance mode 1. Figure 9(a) shows that, while the range of expected conditions is relatively small prior to drag skirt jettison, the range of drag skirt jettison times lead to a much wider range of conditions post-jettison. Figure 9(b) highlights the range of conditions over which the drag skirt is jettisoned. However, similar trends emerge across all trajectories. For this EI-target pair, all jettisons occur after hypersonic peak deceleration (and peak heating). This is due to intentional bias of the jettison point towards the end of the trajectory to improve terminal accuracy; the bias is created by choosing a relatively short target range that forces the vehicle to retain the drag skirt for more of the trajectory. This strategy also reduces peak heat rate and integrated heat load, because the vehicle retains its minimum β through peak heating at approximately 4.8 km/s (Figure 9(c)). This results in a more benign heating environment than that predicted for the MER entries. Specifically, the mean plus 3σ heat rate for this system is over 30% lower than that of MER; integrated heat load is nearly 20% lower.[16] These low heat rates indicate that the heritage SLA561V forebody heat shield material may be used with considerable margin in this EDL architecture. Peak deceleration is similar to that of MER: the reduction in peak deceleration from the more shallow EI flight-path angle used for this trajectory, relative to MER, is largely countered by the decrease in β of the vehicle.[16] Lastly, the step change in sensed deceleration at jettison becomes much smaller as jettison time increases. Late-jettison trajectories maintain a higher altitude for longer, then dive more steeply post-jettison to the parachute deploy point.

Figure 10 shows trajectories for a single drag skirt segment for the mode 1 Monte Carlo simulation data. Again, a C_D of 1.0 was used for the drag skirt segment. The range of drag skirt jettison times leads to a relatively large drag skirt impact footprint (Figure 10(a)). However, Figure 10(b) shows that the minimum separation distance at vehicle touchdown is nearly 20 km, with an average separation distance near 75 km. Additionally, the separation after 3 s is found to be above 100 m, which compares very favorably to the MER requirement for heat shield separation of 21 m in 3 s.[27]

Overall, hypersonic flight performance and drag skirt jettison results were similar for all three guidance modes, as shown in Table 4. All three modes exhibit a more benign heating environment relative to the MER EDL system and preserve at least 70 s of parachute descent time. However, significant differences are present in the parachute deploy conditions and in terminal accuracy.

Significantly, terminal accuracy is competitive with the MSL requirement (within 10 km of the target landing site), even for mode 1. While mode 1 does not satisfy the requirement at touchdown, its mean plus 3σ range error at parachute deploy is only 6.35 km. The mode 1 touchdown range error is larger due to the unaccounted-for bias incurred during parachute descent, which raises the total error to 11.28 km. Modeling the parachute descent, as done in mode 2, effectively removes this bias, reducing the total range error (mean plus 3σ) to 5.54 km, well within the MSL accuracy requirement. The addition of the range-based parachute trigger in mode 3 further improves landed accuracy, with a mean plus 3σ range error of only 3.11 km and a maximum below 5 km. Figure 11 shows the component range error probability density functions for all three modes. Figure 11(a) shows that modeling the parachute descent phase (mode 2) removes the touchdown range bias, but without changing the overall shape of the distribution of range error relative to mode 1. In contrast, adding the range-based parachute trigger (mode 3) reduces the variability of the range error by shrinking the standard deviation. Figure 11(b) shows that crossrange error is approximately constant, with a constant bias of about 0.5 km, regardless of guidance mode. This is the expected behavior, as the vehicle does not possess any out-of-plane control authority. Lastly, Figure 11(c) shows the total touchdown range error cumulative density functions for all three modes,

and highlights the improvements in performance from modeling the parachute descent and including a range-based parachute trigger. Interestingly, the larger improvement comes from modeling the parachute descent. These results indicate that the proposed discrete-event drag modulation EDL system is capable of achieving MSL-class landed accuracy without the addition of thrusters, propellant, tanks, or the complexity of lift modulation, a significant improvement relative to the MER EDL system.

Figure 12 shows the parachute deploy conditions for all three guidance modes. The margined MER parachute deploy criteria are represented by the dashed line, with a dynamic pressure limit of 810 N/m^2. The dotted line represents the MER parachute design limits, with a dynamic pressure limit of 900 N/m^2.[16] Lines of contestant velocity are shown in grey in 10 m/s increments; the parachute deploy velocity (modes 1 and 2) and box (mode 3) are shown as black lines. For modes 1 and 2 (Figure 12(a), the parachute deploy conditions are similar. The margined MER deploy box is exceeded, but the peak dynamic pressure at deploy remains below 850 N/m^2 for both modes, satisfying the MER design limits. Most trajectories deploy slightly below the trigger velocity of 450 m/s because of latency in the control system. The segmentation into two groups of the deploy conditions is also due to control system latency. This latency is the primary cause of error in the deploy velocity; navigation system error is present, but a smaller contributor. Figure 12(b) shows the range of parachute deploy conditions for the range-based trigger. Trajectories are grouped near the deploy box boundaries (also in two groups at each boundary, due to latency). The deploy box velocity boundaries ware chosen to satisfy the MER design limit criteria, and while those criteria are satisfied, little margin exists at the top of the deploy box in either Mach or dynamic pressure. However, small excursions from the accepted DGB flight qualification envelope may be acceptable: the MSL program successfully enlarged its DGB parachute and increased the maximum deployment Mach number.[15] Alternately, a reduction in the size of the velocity deploy box will decrease the range of parachute deploy conditions that must be accommodated at the expense of increasing terminal range error.

DISCUSSION

The results presented indicate that the proposed discrete-event drag modulation EDL architecture is a feasible option for delivering an MER-class payload to the surface of Mars with MSL-class accuracy. The proposed EDL architecture offers significant benefits over traditional bank-to-steer systems in terms of cost and complexity. Relative to MSL, the proposed architecture reduces the number of jettison events and eliminates the need for an off-centerline c.g., propellent, tanks, and RCS on the aeroshell. Relative to MER, the proposed architecture has a more benign aerothermal environment and superior landed accuracy. The proposed system architecture is largely enabled by advances in approach navigation at Mars and onboard computing capabilities. Precise approach navigation reliably provides a narrow range of in-plane EI states and reduces the need for out-of-plane trajectory control. Modern flight computers are capable of running advanced NPC algorithms, which can take advantage of real-time parameter estimation to provide precision guidance and targeting for discrete-event trajectory control systems.

The proposed EDL architecture may be used as a low-risk technology demonstrator for more ambitious drag modulation systems while still landing useful payload on surface of Mars. Drag modulation is easily extensible to the low-β vehicles currently being considered for future high-mass Mars missions. The use of a jettisonable drag area deployed prior to launch significantly reduces risk and allows a technology demonstration mission to focus on entry flight performance

Table 4. Monte Carlo Simulation Results

Parameter	Mean	σ	Mean-3σ	Mean$+3\sigma$	Min.	Max.
Guidance Mode 1: Parachute Deploy Target						
Drag skirt jettison Mach	10.23	2.06	4.04	16.42	3.72	16.45
Parachute deploy altitude, km	5.89	0.41	4.67	7.12	4.63	7.71
Parachute deploy velocity, m/s	447.49	2.27	440.69	454.29	443.97	450.18
Parachute deploy dynamic pressure, N/m^2	760.44	26.16	681.96	838.92	657.33	848.56
Parachute deploy Mach	1.98	0.01	1.95	2.01	1.95	2.01
Parachute deploy range error, km	2.12	1.41	--	6.35	0.07	8.77
Parachute descent time, s	95.24	6.18	76.70	113.78	76.52	115.22
Touchdown range error, km	5.17	2.04	--	11.28	0.82	12.48
Peak deceleration (hypersonic), Earth g	6.06	0.19	5.48	6.64	5.42	6.68
Peak heat rate, W/cm^2	30.16	0.58	28.41	31.91	28.58	31.95
Integrated heat load, J/cm^2	2276	47.7	2133	2419	2180	2466
Guidance Mode 2: Touchdown Target						
Drag skirt jettison Mach	9.24	2.03	3.14	15.34	3.07	15.35
Parachute deploy altitude, km	5.94	0.44	4.61	7.27	4.64	9.02
Parachute deploy velocity, m/s	447.65	2.24	440.94	454.37	443.89	450.25
Parachute deploy dynamic pressure, N/m^2	758.06	28.31	673.14	842.98	574.20	848.37
Parachute deploy Mach	1.98	0.01	1.95	2.01	1.95	2.01
Parachute deploy range error, km	--	--	--	--	--	--
Parachute descent time, s	95.42	6.37	76.30	114.54	76.00	125.88
Touchdown range error, km	1.85	1.23	--	5.54	0.03	7.92
Peak deceleration (hypersonic), Earth g	6.06	0.19	5.48	6.64	5.42	6.68
Peak heat rate, W/cm^2	30.16	0.58	28.41	31.91	28.58	31.95
Integrated heat load, J/cm^2	2251	40.8	2128	2373	2169	2411
Guidance Mode 3: Range-based Parachute Deploy Trigger						
Drag skirt jettison Mach	8.92	2.03	2.83	15.00	2.80	15.00
Parachute deploy altitude, km	5.84	0.65	3.88	7.80	4.20	8.05
Parachute deploy velocity, m/s	445.36	23.80	373.95	516.78	413.73	480.10
Parachute deploy dynamic pressure, N/m^2	755.47	48.29	610.60	900.33	556.50	875.94
Parachute deploy Mach	1.97	0.11	1.64	2.30	1.82	2.14
Parachute deploy range error, km	--	--	--	--	--	--
Parachute descent time, s	93.98	8.91	67.25	120.71	72.65	120.87
Touchdown range error, km	1.10	0.67	--	3.11	0.04	4.96
Peak deceleration (hypersonic), Earth g	6.06	0.19	5.48	6.64	5.42	6.68
Peak heat rate, W/cm^2	30.16	0.58	28.41	31.91	28.58	31.95
Integrated heat load, J/cm^2	2243	38.5	2128	2359	2165	2393

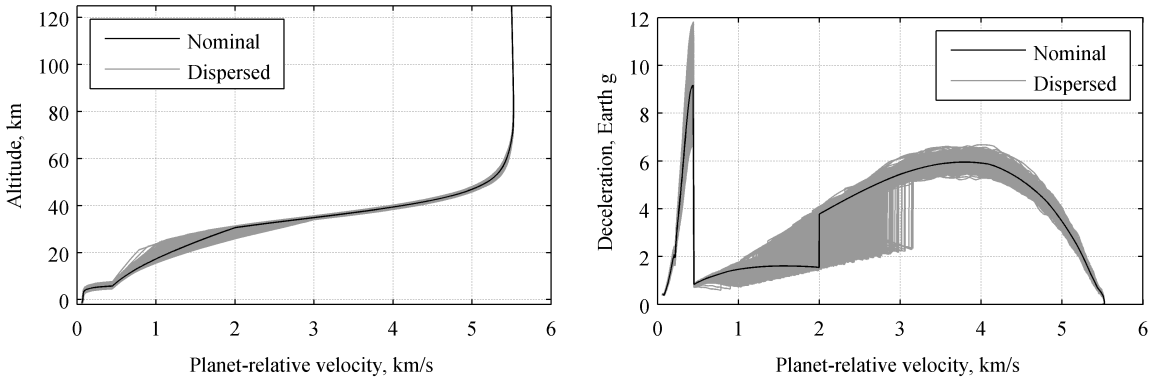

(a) Altitude versus planet-relative velocity.

(b) Sensed deceleration.

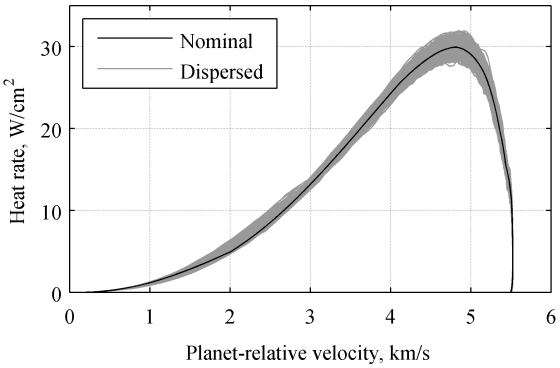

(c) Stagnation-point heat rate.

Figure 9. Dispersed trajectories for guidance mode 1.

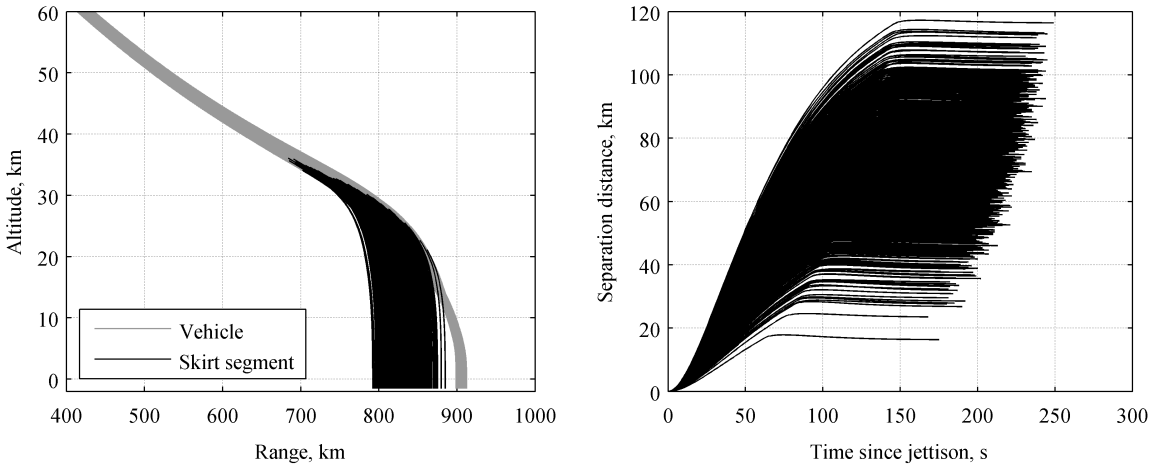

(a) Altitude versus range.

(b) Separation distance.

Figure 10. Post-jettison drag skirt segment trajectories.

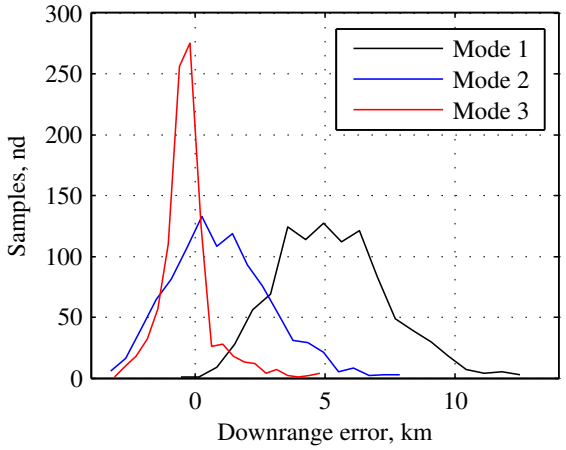

(a) Downrange error probability density function.

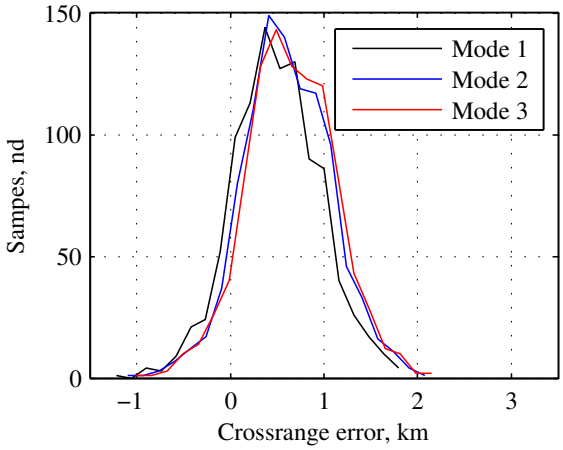

(b) Crossrange error probability density function.

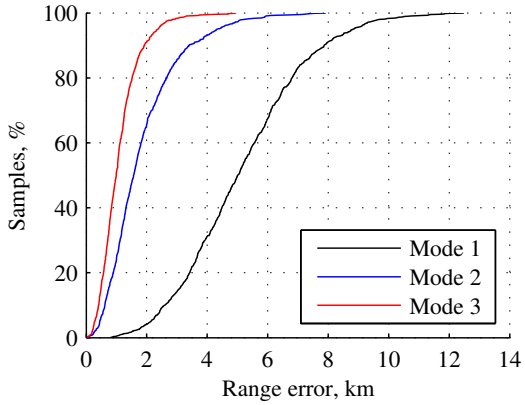

(c) Total range error cumulative distribution function.

Figure 11. Terminal range error for all three guidance modes.

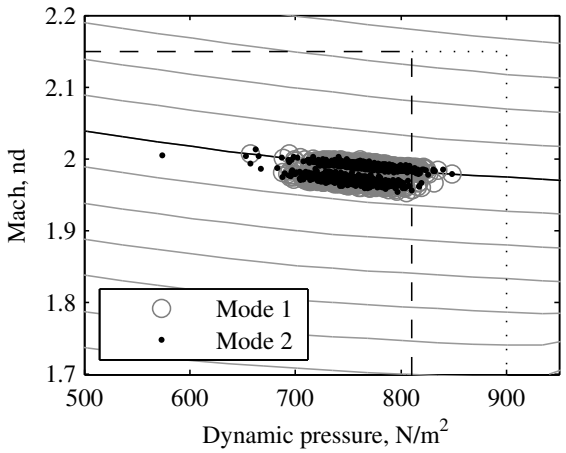

(a) Modes 1 and 2.

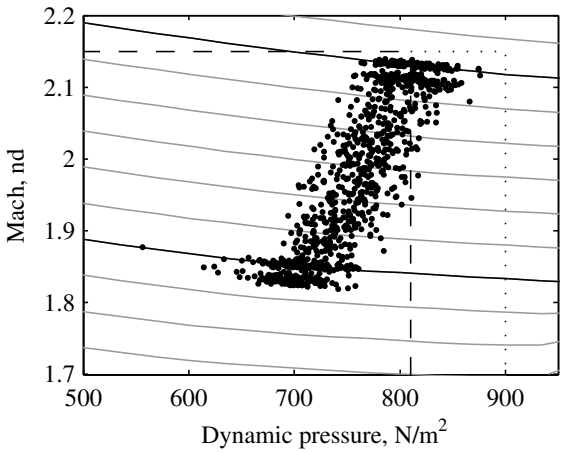

(b) Mode 3.

Figure 12. Parachute deploy conditions.

of the system concept. Drag modulation trajectory control is a prime candidate for use with large, flexible heat shields, such as those envisioned by NASA's hypersonic inflatable aerodynamic decelerator (HIAD) program. The ability to fly at zero angle of attack reduces the criticality of vehicle aerodynamic properties at asymmetric flight conditions; the absence of RCS eliminates concerns about effector latency and jet interaction with a flexible structure and complex wake flow field; the absence of propellant tanks, propellant, and ejectable ballast masses greatly simplifies packaging, system integration, and operational complexity.

However, the proposed discrete-event drag modulation EDL system creates new challenges. First, the jettison must be accommodated over wide range of Mach numbers. While Mach number independence in this regime mitigates this risk, verification and validation approaches have yet to be developed. Second, the proposed drag-only trajectory control concept has less divert capability available to recover from large, unexpected delivery errors. Given that the presence of such large errors can also overwhelm a traditional bank-to-steer system, this is likely a small increase in overall mission risk relative to a traditional bank-to-steer system.

NOTATION

$\mathbf{a}$	acceleration vector, m/s^2	t	time, s
a	acceleration magnitude, m/s^2	$\mathbf{x}$	random vector
C_A	axial force coefficient	x	random variable
C_N	normal force coefficient	$\mathbf{v}$	inertial velocity vector, m/s
C_D	drag coefficient	v_{wind}	wind-relative velocity magnitude, m/s
$\mathbf{e}$	error vector	β	ballistic coefficient, kg/m^2
m	mass, kg	η	Markov process noise
$\mathbf{P}$	covariance matrix	ρ	atmospheric density, kg/m^3
$\mathbf{r}$	position vector, m	σ	standard deviation
S_{ref}	aerodynamic reference area, m^2	τ	time constant, s

ACKNOWLEDGMENT

This work was supported by a NASA Office of the Chief Technologist Space Technology Research Fellowship.

REFERENCES

[1] R. D. Braun and R. M. Manning, "Mars Exploration Entry, Descent, and Landing Challenges," *Journal of Spacecraft and Rockets*, Vol. 44, Mar. 2007, pp. 310–323.

[2] R. Prakash, P. D. Burkhard, A. Chen, K. A. Comeaux, C. S. Guernsey, D. M. Kipp, L. V. Lorenzoni, G. F. Mendeck, R. W. Powell, T. P. Rivellini, R. Sansom, S. W. Sell, A. D. Steltzner, and D. W. Way, "Mars Science Laboratory Entry, Descent, and Landing System Overview," *2008 IEEE Aerospace Conference*, Big Sky, MT, Mar. 2008, pp. 1–18.

[3] M. Schoenenberger, A. Dyakonov, P. Buning, W. Scallion, and J. Van Norman, "Aerodynamic Challenges for the Mars Science Laboratory Entry, Descent and Landing," *41st AIAA Thermophysics Conference*, San Antonio, Texas, June 2009, pp. 1–29.

[4] L. L. Levy, "The Use of Drag Modulation to Limit the Rate at Which Deceleration Increases During Nonlifting Entry," Tech. Rep. NASA TN D-1037, Ames Research Center, Washington, DC, Sept. 1961.

[5] P. H. Rose and J. E. Hayes, "Drag Modulation and Celestial Mechanics," *7th Annual Meeting of of the American Astronautical Society*, Dallas, TX, Jan. 1961.

[6] Z.-S. Kuo, K.-C. Liu, and Y.-S. Chang, "Explicit Guidance of Ballistic Entry Using Improved Matched Asymptotic Expansions," *Transactions of the Japan Society for Aeronautical and Space Sciences*, Vol. 50, Jan. 2007, pp. 121–127.

[7] A. D. McRonald, "A Lightweight Inflatable Hypersonic Drag Device for Planetary Entry," *Association Aeronautique de France Conference*, Arcachon, France, Mar. 1999.

[8] C. H. Westhelle and J. P. Masciarelli, "Assessment of Aerocapture Flight at Titan Using a Drag-only Device," *AIAA Atmospheric Flight Mechanics Conference and Exhibit*, Austin, TX, Aug. 2003, pp. 1–7.

[9] J. L. Hall and A. K. Le, "Aerocapture Trajectories for Spacecraft with Large Towed Ballutes," *AAS/AIAA Space Flight Mechanics Meeting*, Santa Barbara, CA, Feb. 2001.

[10] K. L. Miller, D. Gulick, J. Lewis, B. Trochman, J. Stein, D. T. Lyons, and R. G. Wilmoth, "Trailing Ballute Aerocapture: Concept and Feasibility Assessment," *39th AIAA/ASME/SAE/ASEE Joint Propulsion Conference and Exhibit*, Huntsville, AL, July 2003.

[11] W. R. Johnson and D. T. Lyons, "Titan Ballute Aerocapture Using a Perturbed TitanGRAM Model," *AIAA Atmospheric Flight Mechanics Conference and Exhibit*, Providence, RI, Aug. 2004.

[12] Z. R. Putnam and R. D. Braun, "Drag Modulation Flight Control System Options for Planetary Aerocapture," *51st AIAA Aerospace Sciences Meeting*, Grapevine, TX, Jan. 2013.

[13] R. D. McDaniel, M. J. Wright, and J. T. Songer, "Aeroheating Predictions for Phoenix Entry Vehicle," *AIAA Aerospace Sciences Meeting*, Reno, Nevada, Jan. 2008, pp. 1–25.

[14] T. J. Martin-Mur, G. L. Kruizinga, and M. C. Wong, "Mars Science Laboratory Interplanetary Navigation Analysis," *21st International Symposium in Space Flight Dynamics*, San Jose dos Campos, Brazil, Jan. 2011, pp. 1–15.

[15] D. W. Way, "On the Use of a Range Trigger for the Mars Science Laboratory Entry, Descent, and Landing," *IEEE Aerospace Conference*, Big Sky, Montanta, Mar. 2011, pp. 1–8.

[16] P. N. Desai, M. Schoenenberger, and F. M. Cheatwood, "Mars Exploration Rover Six-Degree-of-Freedom Entry Trajectory Analysis," *Journal of Spacecraft and Rockets*, Vol. 43, Sept. 2006, pp. 1019–1025.

[17] R. D. Braun, R. W. Powell, W. C. Engelund, P. A. Gnoffo, K. J. Weilmuenster, and R. A. Mitcheltree, "Mars Pathfinder Six-Degree-of-Freedom Entry Analysis," *Journal of Spacecraft and Rockets*, Vol. 32, Nov. 1995, pp. 993–1000.

[18] D. A. Spencer and R. D. Braun, "Mars Pathfinder Atmospheric Entry: Trajectory DesignandDispersion Analysis," *Journal of Spacecraft and Rockets*, Vol. 33, Sept. 1996, pp. 670–676.

[19] H. L. Justh and H. S. Ramey, "MARS-GRAM 2010: IMPROVING THE PRECISION OF MARS-GRAM," *4th International Workshop on the Mars Atmosphere: Modelling and Observations*, Feb. 2011, pp. 1–4.

[20] K. Sutton and R. A. Graves, "A General Stagnation-point Convective-heating Equation for Arbitrary Gas Mixtures," Tech. Rep. NASA TR R-376, NASA, Washington, DC, Nov. 1971.

[21] M. E. Tauber and K. Sutton, "Stagnation-point Radiative Heating Relations for Earth and Mars Entries," *Journal of Spacecraft and Rockets*, Vol. 28, June 2003, pp. 40–42.

[22] D. Kinney, "Aero-Thermodynamics for Conceptual Design," *42nd AIAA Aerospace Sciences Meeting and Exhibit*, Reno, Nevada, Jan. 2004, pp. 1–11.

[23] J. R. Cruz, D. W. Way, J. D. Shidner, J. L. Davis, and D. M. Kipp, "Mars Science Laboratory: Description of the Parachute Models Used in the POST End-to-end Simulation," tech. rep., NAS, July 2012.

[24] S. A. Striepe, D. W. Way, and A. M. Dwyer, "Mars Science Laboratory Simulations for Entry, Descent, and Landing," *Journal of Spacecraft and Rockets*, Vol. 43, Mar. 2006, pp. 311–323.

[25] T. Vincenty, "Direct and Inverse Solutions of Geodesics on the Ellipsoid with Application of Nested Equations," *Survey Review*, Vol. XXII, Apr. 1975, pp. 88–93.

[26] R. A. Mase, D. A. Spencer, J. C. Smith, and R. D. Braun, "Navigation Stragtegy for the Mars 2001 Lander Mission," *AAS/AIAA Astrodynamics Specialist Conference*, Girdwood, AK, Apr. 2001, pp. 1–16.

[27] B. Raiszadeh, P. N. Desai, and R. Michelltriee, "Mars Exploration Rover Heat Shield Recontact Analysis," *21st AIAA Aerodynamic Decelerator Systems Technology Conference and Seminar*, Dublin, Ireland, May 2011.